Received: February 13, 2021. Revised: March 10, 2022. 281

International Journal of
Intelligent Engineering & Systems

http://www.inass.org/

# Novel Approach of Constant Switching Frequency MPC for 3L-NPC Converter-Based PMSG Wind Energy Conversion Systems with LVRT Capability

**Asmaa A.Ghany[1,2]* Ahmed A. Zaki Diab[1] Abo - Hashima M. Elsayed[1]**
**Yahia S. Mohamed[1] E. G. Shehata[1]**

[1]*Department of Electrical Engineering, Minia University, Minia 61111, Egypt*
[2]*Department of Electrical Engineering, Beni - Suef University, Beni - Suef 62521, Egypt*
* Corresponding author's Email: asmaamohamed@eng.bsu.edu.eg

**Abstract:** Nowadays, great attention has been paid to wind energy conversion systems (WECS), particularly high-power stations equipped with high-power electronic converters. Direct-driven permanent magnet synchronous generator (PMSG) with three-level converters is the preferred type for such wind energy systems. To regulate the operation of the generation system, a finite control set model predictive control (FCS-MPC) has a superior performance for power converters control techniques due to tight control dynamics, simple design, multi-variables control, no modulation control stage, and only a discrete-time model is needed. But on the contrary, variable switching frequency output waveforms is the main drawback. The main objective of the paper is to design a controller of a three-level neutral point clamped (3L-NPC) converter with a novel fixed switching frequency for regulating the stator current of PMSG and ensure the balance of the DC-link capacitors voltages. In addition, a low voltage ride-through (LVRT) control technique is provided for the grid side converter of the wind power system to improve the wind turbine system performance throughout the grid fault. The futured system has been demonstrated via simulation work under steady states, transient conditions, and different types of grid voltage faults. The comparative results between MMPC and classical FCS-MPC show the effectiveness of the proposed MMPC in enhancing the results and reducing the simulation execution time and the computational effort associated with the calculation of the duty cycle of the converters also the total harmonic distortion (THD) has reduced by 31.34% lower than classical FCS-MPC and obtaining a constant switching frequency with a reduction in execution time by 51.17%. In addition, the comparative results of WECS during symmetrical and asymmetrical grid faults with and without LVRT controller show the effectiveness of LVRT controller in supporting the grid during faults and preventing the dc capacitor overvoltage.

**Keywords:** Permanent magnet synchronous generator, Three-level neutral point clamped inverter, Model predictive control, Low voltage ride through.

## 1. Introduction

Recently, considerable attention has been paid to wind energy, particularly high-power wind stations. Nowadays, 7.5 MW are accessible in the market, and research activities focus on installing 12 W plants for offshore applications [1-4]. Such a trend makes multilevel voltage converters play a vital role in dealing with these high ratings of power and achieving grid code requirements (GCRs). The total harmonic distortion and switching losses of large power electronics units must be minimal [4].

Direct-driven permanent magnet synchronous generator (DDPMSG) wind energy system is extensively used in wind power generation due to advantages like high efficiency, gearbox elimination, low maintenance, and compact size [5]. So, three-level neutral point clamped (3L-NPC) back-to-back converters seems a good selection for high-power wind turbine system [6, 7]. These converters can be operated as a machine-side converter (MSC) and grid-side converter (GSC). Several advantages for 3L-NPC such as low harmonic distortion and lower voltage stress on dc-link capacitors. It can operate at

a low switching frequency which makes it more dominant in high power industrial applications. Controlling the MSC and GSC to achieve optimum performance of the generation system under normal and abnormal conditions is one of the main topics in variable speed wind energy systems.

Under normal operating conditions, different control systems like field-oriented control, direct power control, and model predictive control are applied for power converters. Several studies considered that Finite control-set model predictive control (FCS-MPC) is a more appropriate non-linear control technique. It has many essential benefits, such as simple design, fast control dynamics, and it is considered a promising tool for power converters control. However, the major drawback of this approach is high computational load, particularly for multilevel [8, 9]. To solve these problems, modern digital implementations (e.g., FPGA, Microprocessor, and DSPs) have provided a good solution for real-time implementation [10-14]. To solve this issue, [10] has proposed a new technique called modulated predictive model control (MMPC) to control both the load current and dc-link capacitor voltages of the NPC converter. While [11] applied this method to improve the power quality of DFIG and obtain a fixed switching frequency operation. But the drawback of the above approaches is that they operate at a high switching frequency.

Since FCS-MPC has attracted much attention and has superior performance as it applies only one voltage vector during the whole sampling time, its control produces variable switching frequency output waveforms. Variable switching frequency causes the converter to produce large harmonic content, so the power quality of the system will also degrade. In [11], an FCS-MPC with an indirect power control scheme has been proposed for a doubly-fed induction generator controlled with a matrix converter for achieving fixed switching frequency operation. The stator current harmonic spectrum has been reduced. Also, the active and reactive grid power ripples have been enhanced as the reported results. In [12], a deadbeat predictive controller for switched reluctance machine to calculate the duty cycle of the PWM pulses for whole operating speed. In [13], the predictive control for current error and switching frequency minimization has been studied. References [14-16] indicate a fixed switching period of PWM with the triangular carrier, which uses small evaluation steps to enhance the performance of power converters. Fixed switching frequency has also been discussed by [17, 18], but switching time calculations are very complicated, so it becomes difficult to add constraints in the cost function.

Under abnormal grid voltage conditions, and to reserve the generation system connected to the grid even under grid faults, LVRT capability has been considered an important technique. LVRT technique is provided for the grid side converter to adjust the grid reactive power hence reactive current during a three-phase fault. A mismatch appears among the active power generated and the one delivered to the grid during a fault, so the LVRT technique should protect the DC-voltage from overvoltage during and after grid fault [19]. When the grid voltage sags, WT is required to remain connected to the grid, and this is critical for the grid integration of WPS. Electric utilities have their own grid codes identified as grid code requirements (GCR) which establish grid criteria during grid voltage occurrence [20]. This grid code often covers a wide variety of topics, including power factor regulation, grid support capability, frequency operating range, and low voltage ride through (LVRT). When grid voltage drops, the LVRT requirements require WPS to stay connected to the network by providing active and reactive power to the electric grid with a specified profile depending on the voltage dip. As a result, the LVRT criteria is the most significant of the GCR. During a grid failure, the grid side converter (GSC) is unable to transfer all of the power from the machine side converter (MSC) to the grid. As a result of the power mismatch between MSC and GSC, The DC bus voltage rises dramatically and the WECS will lose its stability. Furthermore, overcurrent and overvoltage appear on the converters, which triggers the system protection and isolates the system from the grid [21]. A Kalman observer controller coupled to crowbar and braking chopper circuits has been applied in [22] to ride through grid faults by estimating the generated power of the DFIG but it did not study a symmetrical grid voltage fault.

This paper is to construct a novel cost function algorithm with a time pattern to make the switching frequency of the converter constant where the duty cycles have been computed based on the cost functions of selected vectors. In addition, the control algorithm will operate at a certain extent low switching frequency keeping dc-link capacitor voltages balanced. This paper also introduces a LVRT technique to enhance the system stability during grid voltage dip and protect the dc-link voltage from overvoltage. The simulation results will prove that the LVRT algorithm and the operation at a fixed switching frequency will improve the PMSG capability during transient and steady-state operation. The paper contributions can be summarized as follows:

- Overcoming the variable switching frequency of the three-level converter problem by designing a modulation algorithm that obtains a fixed switching frequency, where a cost function algorithm with a time pattern to make the switching frequency of the converter constant has been proposed.
- The application of the novel cost function aids the control algorithm to operate at a certain extent low switching frequency and keeping dc-link capacitor voltages balanced.
- A comparison between the classical FCS-MPC and Modulated Model Predictive control (MMPC) techniques to show the contribution of the MMPC in the performance of WECS.
- A LVRT technique has been applied to enhance the system's stability during symmetrical and asymmetrical grid faults.

The rest of the paper has been structured as follows: Section 2 describes the system modelling and description of PMSG. Section 3 introduces the conventional MPC method for 3L-NPC, the proposed model predictive control for stator current, and dc-link capacitor voltages balancing, and also LVRT capability. Section 4 discusses the simulation results for different operating conditions and different types of grid voltage faults. Finally, the conclusion is reported in Section 5.

## 2. System modelling and description

A direct-driven PMSG WECS involves of a wind turbine directly connected to PMSG without any gearbox, Machine side power converter, DC-link capacitors, Grid side power converter tied to the grid, and the block diagram of these components has been displayed in Fig. 1. In this study, the power converters are 3L-NPC back-to-back converters, and voltage-oriented control with PI regulator has been implemented for the grid-side converter. GSC regulates the injected active/reactive power into the grid and reserves DC-link voltage at the desired value during normal/abnormal conditions. MSC is controlled using MPC to regulate the stator current of PMSG to achieve maximum power point tracking. For the following quantities used in the system, $X_{\alpha\beta}$ denotes to variables in αβ stationary reference frame, $X_{dq}$ denotes variables in $dq$ rotating reference frame [23].

### 2.1 Wind turbine power control

Depending on the wind speed ($v_w(m/s)$)which is obtained from the anemometer, maximum power can only be extracted when the turbine operates at maximum power coefficient ($C_p$) and optimum tip speed ratio ($\lambda_T$); i.e., pitch angle β=0 and it can be written as

$$P_m = 0.5\,\rho\,A\,C_p\left(\frac{R_T}{\lambda}\right)\omega_m^3 \tag{1}$$

$\rho$: the air density in ($kg/m^3$), A: rotor area in ($m^2$)
$\omega_m$: the generator speed in ($rad/s$) which produce optimum power and can be obtained from the following formula [24].

$$\omega_m = \frac{\lambda}{R_T}\,v_w \tag{2}$$

When the wind speed reduces below the cut-in speed, the turbine will not operate for generating any power. But if the wind speed increases above this value and reaches its rated one, the turbine will operate at maximum $C_p$ and maximum power will be obtained. Any further increase in wind speed will make the control system force the turbine to operate at rated speed by changing pitch angle. When the wind speed reaches cut-out speed, the control reduces the pitch angle and shuts down the turbine. Detailed explanations of MPPT can be found in [25].

### 2.2 Permanent magnet synchronous generator mathematical model

A surface-mounted permanent magnet synchronous generator mathematical equation in $dq$ frame can be expressed using the state-space model. where the stator inductances are equal i.e., $L_d = L_q = L_s$ and taking $i_d^* = 0$ for maximum torque per ampere control (MTPA) [29].

$$X(k+1) = A(k)X(k) + B(k)u(k) + H(k) \tag{3}$$

where $X(k)$ denotes the stator current $i_{dq}(k)$, $u(k)$ denotes the stator voltage $v_{dq}(k)$. Moreover, the $A(k), B(k)\ and\ H(k)$ can be defined as the following:

$$A(K) = \begin{bmatrix} 1-\frac{R_s}{L_s}T_s & T_s\omega_e(k) \\ -T_s\omega_e(k) & 1-\frac{R_s}{L_s}T_s \end{bmatrix}$$
$$B(k) = \begin{bmatrix} \frac{T_s}{L_s} & 0 \\ 0 & \frac{T_s}{L_s} \end{bmatrix}, H(k) = \begin{bmatrix} 0 \\ -\frac{T_s}{L_s}\varphi_m\omega_e(k) \end{bmatrix} \tag{4}$$

where $R_s, L_s$ are the stator resistance and inductance, respectively.

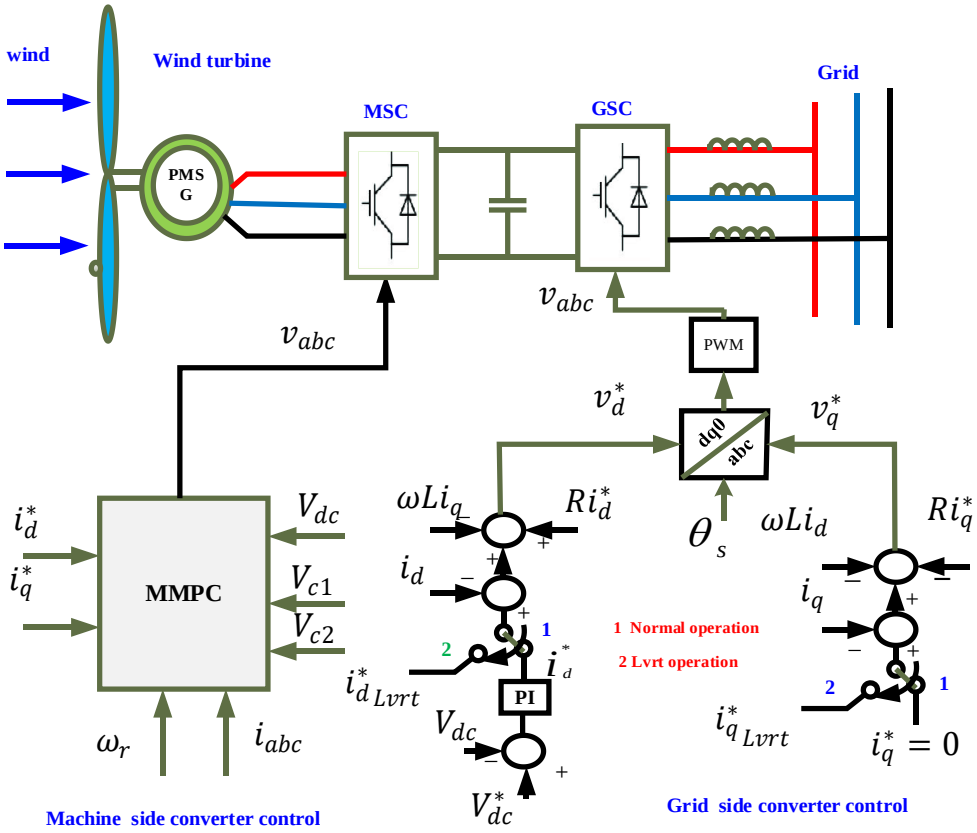


Figure. 1 Block diagram and control structure of PMSG-WECS

$\varphi_m, \omega_e$ are the flux linkage and electrical frequency, $T_s$ sampling time.

### 2.3 Three-level NPC converter topology and modelling

Fig. 2 shows the space vector diagram of 3L-NPC where a 27-switching state and 19 voltage vector $(u_x)$ are available for that converter, and we can define the switching state $(s_x)$ and it's complementary $(\bar{s})$ where $x = a, b, c$.

$$u_x = \begin{cases} P \;\; if \; s_{1x} = 1, s_{2x} = 1 \\ O \;\; if \; s_{1x} = 0, s_{2x} = 1 \\ N \;\; if \; s_{1x} = 0, s_{2x} = 0 \end{cases} \quad (5)$$

So, the converter three-phase voltage with respect to the neutral point (N) of the dc-bus can be formulated depending on the dc-link capacitor voltage and the switching states.

$$V_{xN} = \frac{V_{c1}+V_{c2}}{6}.T_{sw}.u_x + \frac{V_{c1}-V_{c2}}{6}.T_{sw}.|u_x| \quad (6)$$

where $T_{sw} = \begin{Bmatrix} 2 & -1 & -1 \\ -1 & 2 & -1 \\ -1 & -1 & 2 \end{Bmatrix}$ and $V_x$ is in $abc$ coordinate.

For digital controller implementation, a discrete-time model using forward Euler approximation should be defined for dc-link capacitor voltage representation at sampling time $T_s$ and instant time $(k)$ [23].

$$\frac{dV_{cx}}{dt} = \frac{V_{cx}(k+1)-V_{cx}(k)}{T_s} \quad (7)$$

$$V_{c1}(k+1) = V_{c1}(k) + \frac{T_s}{C} i_{c1}(k) \quad (8)$$

$$V_{c2}(k+1) = V_{c2}(k) + \frac{T_s}{C} i_{c2}(k) \quad (9)$$

$i_{c1}(k), i_{c2}(k)$ depend on the converter switching states that can be formulated as follows

$$i_{c1}(k) = i_{dc}(k) - i_a(k)s_{1a} - i_b(k)s_{1b} - i_c(k)s_{1c} \quad (10)$$

$$i_{c2}(k) = i_{dc}(k) - i_a(k)s_{2a} - i_b(k)s_{2b} - i_c(k)s_{2c} \quad (11)$$

where $i_{dc}$ denotes the dc link capacitor current.

For capacitor voltage balancing, the voltage difference $V_{c1} - V_{c2}$ should be kept zero all the time and under any operating condition. So, its control can be obtained from the machine side converter or the

grid side converter. In this study, the machine-side converter achieves the balance, as mentioned in the following section.

## 3. Proposed control algorithm

In this section, the model predictive has been designed and analysed. An overview of the classical model predictive control has been presented in subsection 3.1. while the novel FCS-MPC-based, the novel objective function has been introduced in subsection 3.2.

### 3.1 Classical model predictive control

Classical FCS-MPC is a well-known control method that utilizes a finite (admissible) number of switching states generated by the converter, which are used to predict the future behaviour of the control objectives at each switching state. Then, a cost function is evaluated from the reference of the control objectives with respect to their predictions for the 27 switching states, and the one that achieves minimum cost function is selected and assigned as the optimum gating signal and applied to the converter [10]. A cost function that combines two control objectives; stator current and dc voltages balancing, is represented as follows:

$$g = |i_\alpha^* - i_\alpha(k+1)|^2 + \left|i_\beta^* - i_\beta(k+1)\right|^2 + \lambda_{dc}|V_{c1}(k+1) - V_{c2}(k+1)|^2 \quad (12)$$

where $\lambda_{dc}$ denotes the weighting factor of dc capacitor voltage balancing. The overall structure of this control for the machine-side converter has been described in Fig. 3(a). Since classical FCS-MPC utilizes only one voltage vector during each sampling time that enlarge the computational load, especially for long step predictions, the output current contains much more ripples and the THD spectrum spreads over a wide range resulting in a variable switching frequency operation and this will be shown from the profile of the stator current and THD spectrum results.

***Remark 1*** tuning of weighting factor basically exists when there is an objective control term of cost function more important and needs further optimum performance than the other term. So, for equal importance of both objectives, the weighting factor is set here to 1.

### 3.2 Modulated model predictive control (MMPC)

For the NPC converter space vector diagram in Fig. 2, it is possible to define 24 regions where each region can be adjusted using two active and one zero

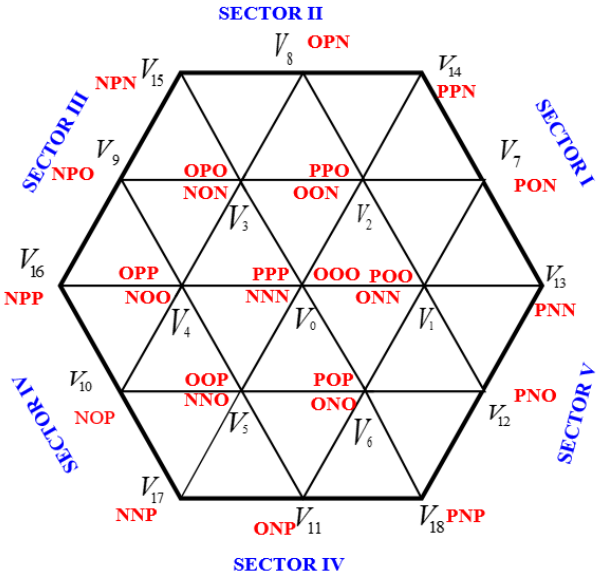


Figure. 2 Space vector diagram of 3L-NPC

voltage vector. For example, the first sector is the one between voltage vectors $V_1, V_2, V_0$ which are generated by switching states based on Eqs. (5) and (6). Since classical FCS-MPC utilizes only one voltage vector during each sampling time, the output current contains much more ripples and the THD spectrum spreads over a wide range resulting in a variable switching frequency operation.

The proposed MMPC overcomes the above-mentioned problems as it produces constant switching frequency, as will be presented in this subsection. Fig. 3(b) demonstrates the strategy of MMPC for the machine side converter, which is similar to classical FCS-MPC as it applies the predicted values of machine stator current and capacitor voltages in Eqs. (3), (7) to and (9). Moreover, the proposed algorithm evaluates a cost function from the voltage vectors of each sector depending on Eq. (13); i.e., for sector one, $g_{1a}, g_{1b}, g_{1c}$ are the cost functions of vectors $V_1, V_2, V_0$ respectively at each sampling time, and the cost function for sector one is defined as:

$$G_1 = \frac{3}{\frac{1}{g_{1a}} + \frac{1}{g_{1b}} + \frac{1}{g_{1c}}} \quad (13)$$

This process is repeated for each sector, and the minimum $G$ is selected as the optimum and applied to the converter, but before this step, the operating time for the selected region is evaluated as [1]:

$$t_{1a} = T_s \frac{g_{1b}g_{1c}}{g_{1a}g_{1b} + g_{1b}g_{1c} + g_{1c}g_{1a}} \quad (14)$$

$$t_{1b} = T_s \frac{g_{1a}g_{1c}}{g_{1a}g_{1b} + g_{1b}g_{1c} + g_{1c}g_{1a}} \quad (15)$$

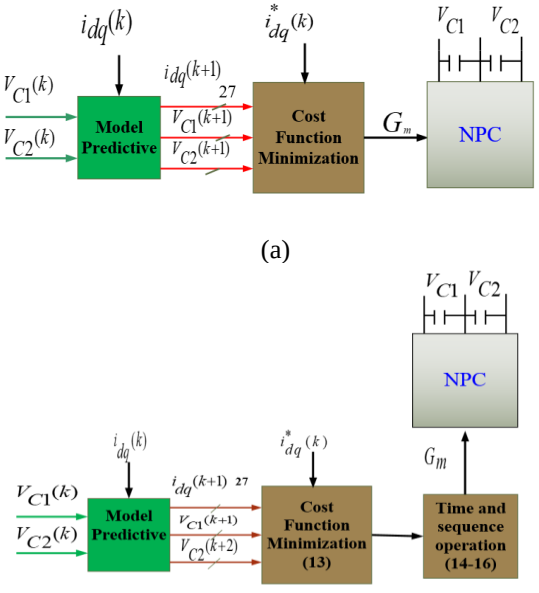


Figure. 3 Block diagram of (a) Classical FCS-MPC system and (b) Proposed MMPC for machine-side converter

$$t_{1c} = T_s \frac{g_{1b}g_{1a}}{g_{1a}g_{1b}+g_{1b}g_{1c}+g_{1c}g_{1a}} \tag{16}$$

A switching pattern procedure depicted in Fig. 4 is formed from these expressions to apply the selected voltage vector.

***Remark 2*** note that a similar approach for modulated model predictive control has been addressed in [11] using matrix converter for rotor current control only and in [10] for 3L-NPC converter with weighting factor in the cost function, but this paper has been extended the grid-tied PMSG-WECS with not only stator current control but also capacitor voltages balancing without inserting weighting factor in the cost function.

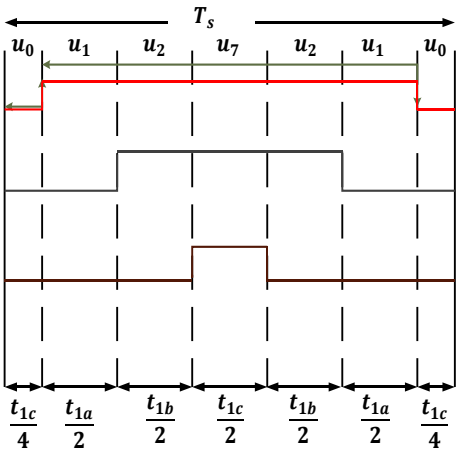


Figure. 4 Switching pattern of voltage vectors

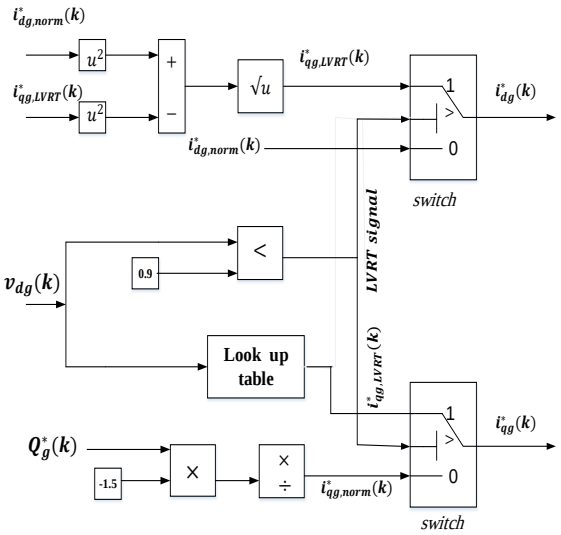


Figure. 5 LVRT algorithm for grid side converter control

### 3.3 Control algorithm of LVRT operation for GSC

Due to increasing wind power penetration into the grid, grid code requirements (GCRs) are continuously updated [26]. LVRT is an essential issue for WECS as the system must keep in operation despite grid faults such as grid voltage dip (GVD), where reduces grid active power resulting in a surplus power across dc-bus capacitors due to high input mechanical power, and this will cause over-current at the grid side. Since over-current is harmful to WECS, the operation should be kept continuous during GVD, and reactive power should be injected into the grid to make it be able to recover its normal operation [27]. Fig. 5 shows the generation of $dq-axis$ reference currents for the grid-side converter during LVRT operation depending on E-ON German code.

When a grid voltage dip appears, power should be supplied to the grid. So, reactive power hence reactive current ($i^*_{qg,Lvrt}$) should be injected into the grid to hold the grid voltage and support the network. This current value depends on the amount of grid voltage reduction, which is determined from a lookup table (see Fig. 5). This control strategy must occur within a certain time, for instance, $20\,msec$ according to E-ON German code. Another protection circuit topology called the crowbar circuit is also used to protect the PMSG stator voltage from overvoltage during grid fault and can keep the dc bus voltages balanced by dissipating excess energy in a resistor. This circuit consists of a power electronic device (IGBT) connected in series with a DC resistor and placed parallel to the dc capacitors. The behaviour of this circuit and the effect of the value of the resistance on the dc bus voltages is studied in [28]. In this paper, the grid side converter combined with the crowbar

protection circuit will be studied and simulated for comparison.

## 4. Simulation results and discussion

The simulation results of the proposed modulated model predictive control and LVRT of PMSG WECS, which are validated using MATLAB/Simulink software package, have been presented. Different working conditions, including normal and abnormal, are also tested, considering a one-step prediction horizon for all the results of the suggested MMPC method and an execution sampling time of Ts=50 µs.

Four scenarios have been studied for evaluating the performance of the control system during different wind speed and grid voltage dips. The scenarios can be considered as follows:

- **Scenario I:** Variable wind speed conditions.
- **Scenario II:** Symmetrical three-phase grid voltage dip without LVRT control.
- **Scenario III:** Symmetrical three-phase grid voltage dip with LVRT control.
- **Scenario IV:** Asymmetrical three-phase grid voltage dip.

### 4.1 Scenario I: Variable wind speed conditions

Despite the gradual change of wind speed, a step change is applied here in Fig. 6 to demonstrate the reliability of the proposed MMPC algorithm under different working conditions. Generator speed presents in Fig. 6(b) where it still tracks the abrupt changes of wind speed in a stable manner while the wind speed variations are reflected in grid active power waveform as overshoot and dip in its magnitude during the increase and decrease in its value, respectively. But grid reactive power is kept at zero Fig. 6(c). however, there is a very small overshoot and dip in dc bus voltage at the time of wind speed variation. Additionally, the capacitor voltages are kept balanced by the controller, with a negligible difference between $V_{c1}$ and $V_{c2}$ as denoted in Fig. 6(d).

For the sake of comparison, traditional FCS-MPC has been implemented for machine-side converter during abnormal operating conditions. According to Fig. 7, the FCS scheme has good transient response operations in both grid power and capacitor voltages. However, the major drawback of this approach is high computational load, particularly for multilevel. Since in the traditional FCS scheme, only one voltage vector is applied in each sampling time, a variable switching frequency will occur, and its increase will contribute to changes in the PMSG stator current. So, by considering MMPC scheme, the drawback of the variable switching frequency will be eliminated as the concept of this technique is applying two actives

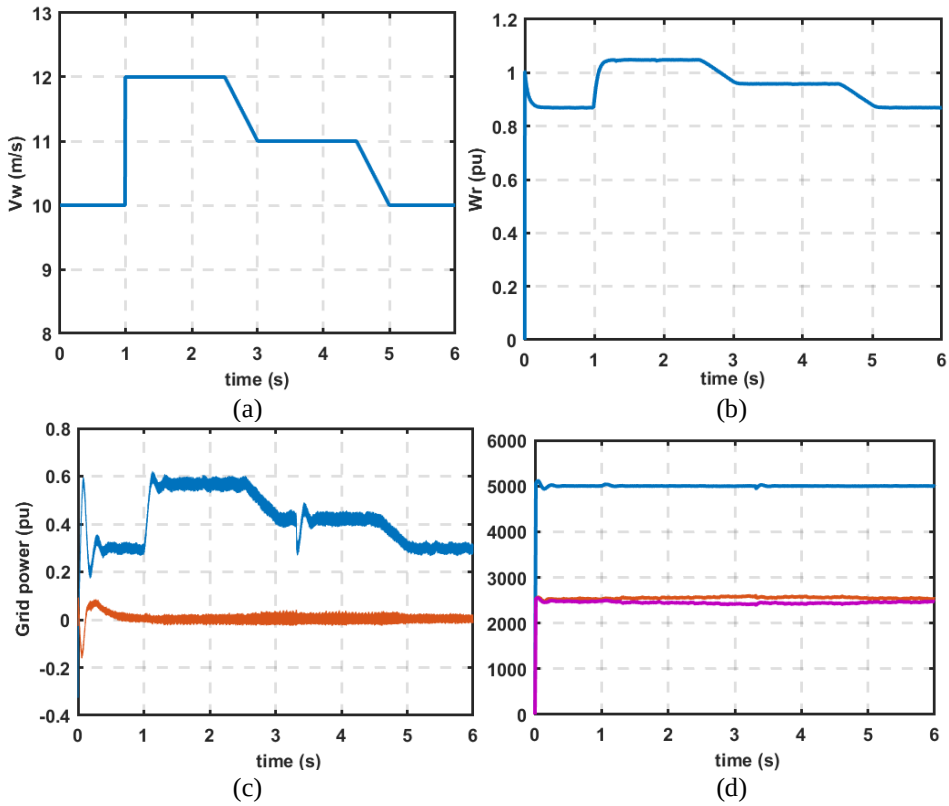


Figure. 6 Simulation results of MMPC at sudden changes of wind speed: (a) Wind speed, (b) Generator speed, (c) Grid power, and (d) Capacitor voltages

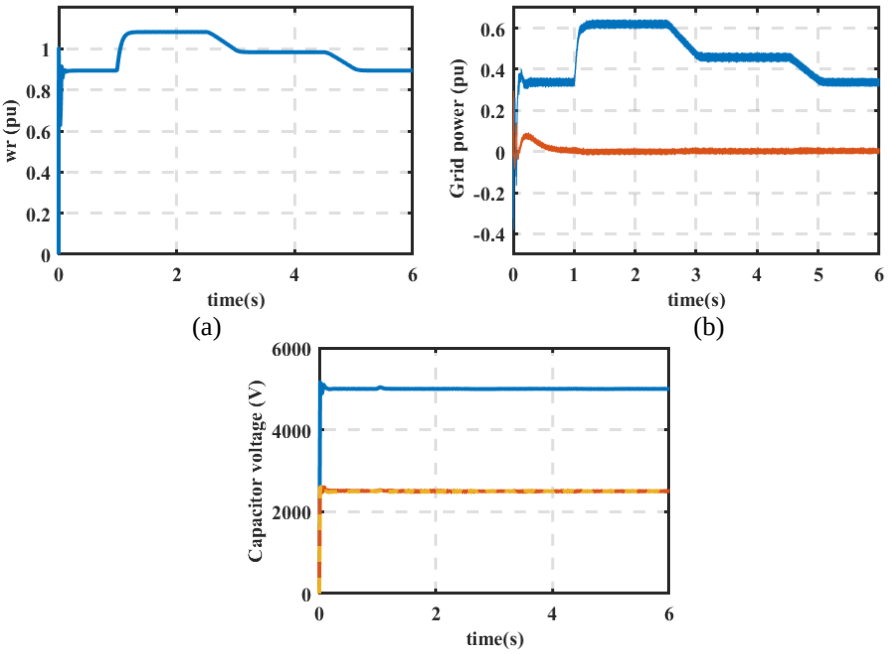


Figure. 7 Simulation results of FCS-MPC at sudden changes of wind speed: (a) Generator speed, (b) Grid power and (c) Capacitor voltages

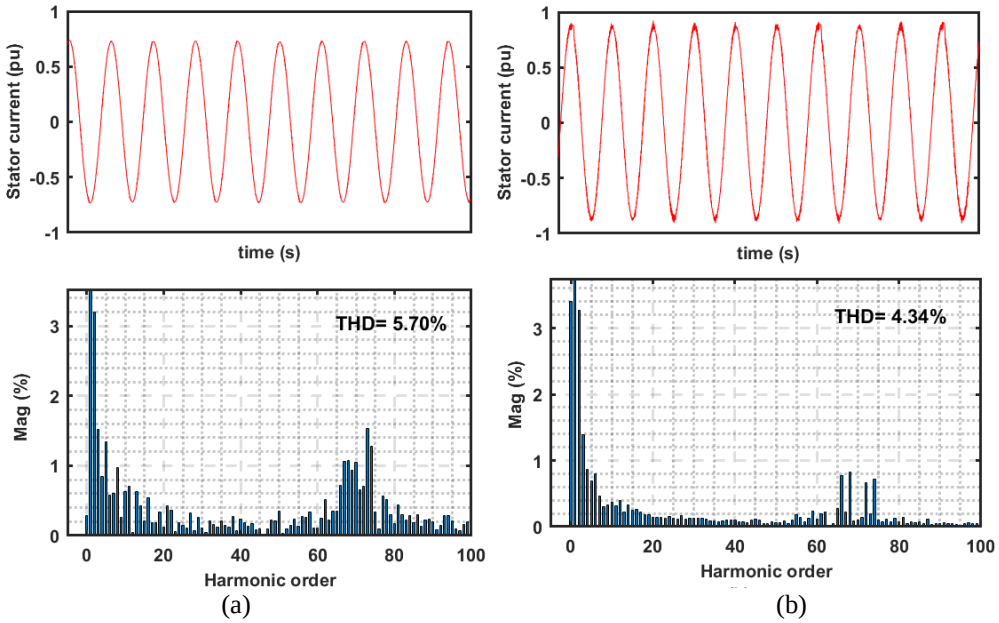


Figure. 8 Stator current and THD: (a) with FCS-MPC and (b) with MMPC

and one zero vector at each sampling time, and their corresponding duty cycle is calculated from a cost function.

Stator currents during both FCS and MMPC with their FFT analysis are outlined in Fig. 8 where nearly sinusoidal voltage waveform and much less ripples are observed, resulting in a lower stator current THD of 4.34 % compared to traditional FCS, which has THDof 5.7% and a more concentrated spectrum which ensures that the proposed MMPC scheme operates at the fixed switching frequency.

To better illustrate the comparison results, the aspects of both presented methods in terms of their THD, total execution time of simulation, and controller and reduction in time required as listed in Table 1. Since in the conventional FCS-MPC, only one voltage vector is applied during the whole sampling time, which results in a variation in switching frequency. The proposed MMPC applies

Table 1. Summarized valuation

| | FCS-MPC | MMPC |
|---|---|---|
| THD% | 5.70% | 4.34% |
| Simulation execution time in (s) | 39.67 | 160.98 |
| Controller execution time in (s) | 1.5468 | 0.7553 |
| Reduction in time (%) | 51.17% | |

two active and one zero voltage vectors during the sampling time based on the switching pattern in Fig. 4. Thus, the computational efforts associated with the calculation of duty cycle are smaller than the conventional FCS-MPC because of the reduction in simulation and controller time.

### 4.2 Scenario II: Symmetrical three-phase grid voltage dip without LVRT control

Symmetrical three-phase fault is applied to the proposed system under fixed wind speed at $t = 1\ sec$ with a duration of $0.5\ s$ and a depth of $90\%$. The following presented results of Fig. 9 are obtained when the LVRT controller is disabled during fault interval, and the grid current increases during fault and then backs to its normal after fault clearance Fig. 9(a) and 9(d) since active power delivered to the grid has reduced to zero with the existence of GVD. Also, the mechanical power from the generator will cause an overvoltage across the parallel-connected capacitors that may damage and destroy them. These results are shown in Fig. 9(e). Moreover, a zoom-out of capacitor voltages during fault duration is depicted in Fig. 9(f). Since the surplus power from the generator had appeared as an overvoltage across capacitor voltages, the generator speed did not change during GVD, as shown in Fig. 9(b).

### 4.3 Scenario III: Symmetrical three-phase grid voltage dip with LVRT control

For the reasons mentioned above and to avoid these problems, the previous test is repeated while enabling LVRT controller during GVD. The results of such a case of study can be observed from Fig. 10(a) and 10(b) both grid active power and current are reduced to zero since the applied fault is more than $50\%$ dip below rated grid voltage, so the LVRT controller should supply the grid with rated reactive current to support it and to limit the dc capacitors voltages to safe values as illustrated in Fig. 10(c) and 10(d). after fault clearance, the controller quickly returns the system to its normal pre-fault condition. So, the simulation results indicate a reliable system under GVD operation.

### 4.4 Scenario IV: Asymmetrical three-phase grid voltage dip

In this case, the voltage of phase a has dropped to $0.1$ pu at $t = 2$ sec and lasts for $0.625$ sec while phases b and c remain at 1 pu as depicted in Fig.11(a). Since during asymmetrical three-phase fault, negative sequence component appears in the grid current distorting both grid power and the electromagnetic torque of the generator, the control of this component becomes much more important and indispensable. However, the details of this control are

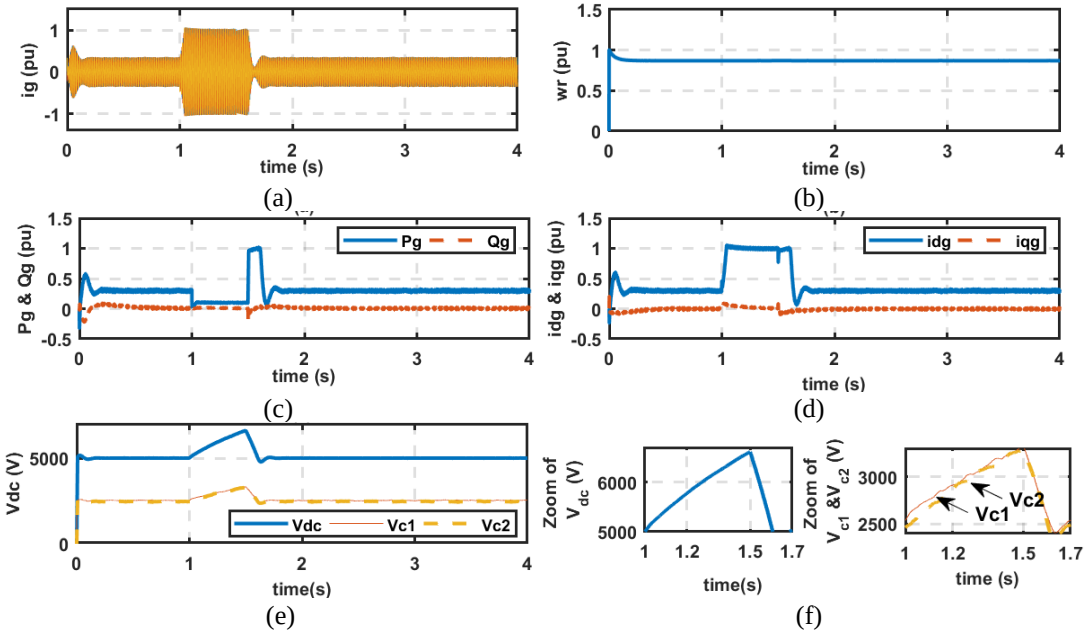


Figure. 9 Simulation results during GVD when the LVRT controller is disabled

out of the scope of this paper. Fig. 11(b) exhibits the grid active power, which drops to zero due to fault occurrence, so the LVRT controller injected a reactive current of about 0.55 pu and hence a reactive power to the grid corresponding to the grid code requirements through fault time as shown in Fig. 11(c). The injected reactive current helps the dc-link capacitor voltages to keep within the acceptable ranges with an acceptable fluctuation during the fault time as depicted in Fig. 11(d) and their zoomed ones. The slow response of the grid current and power is due to the controller used for eliminating the negative sequence component, which can be improved in future work.

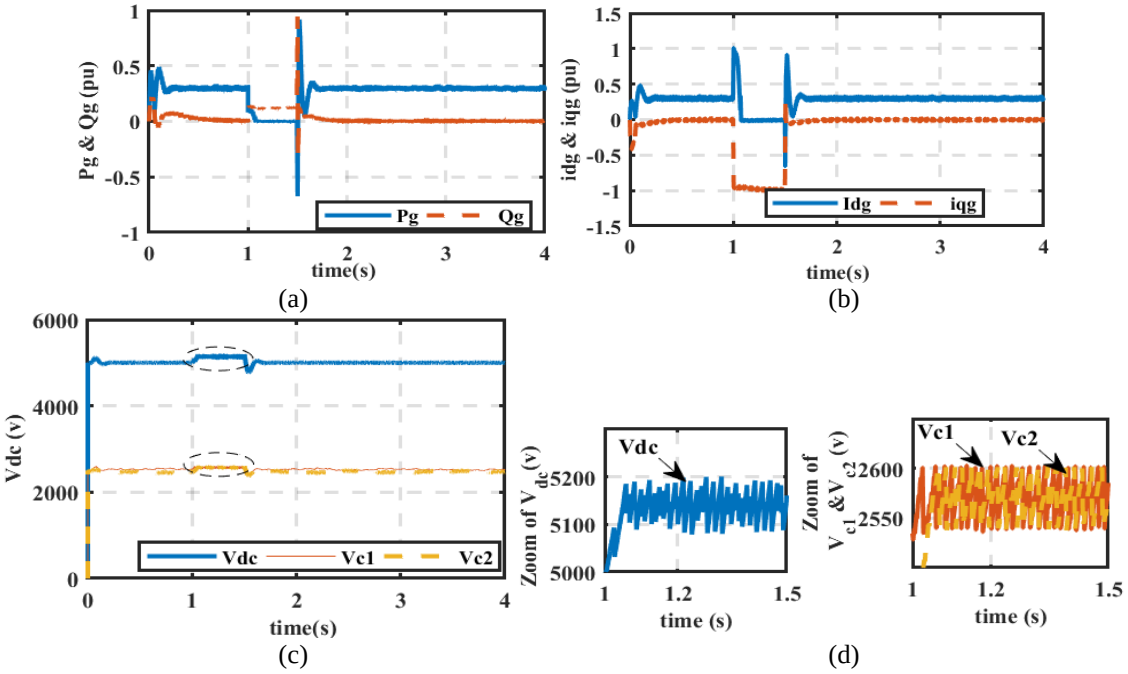


Figure. 10 Simulation results during GVD when the LVRT controller is applied

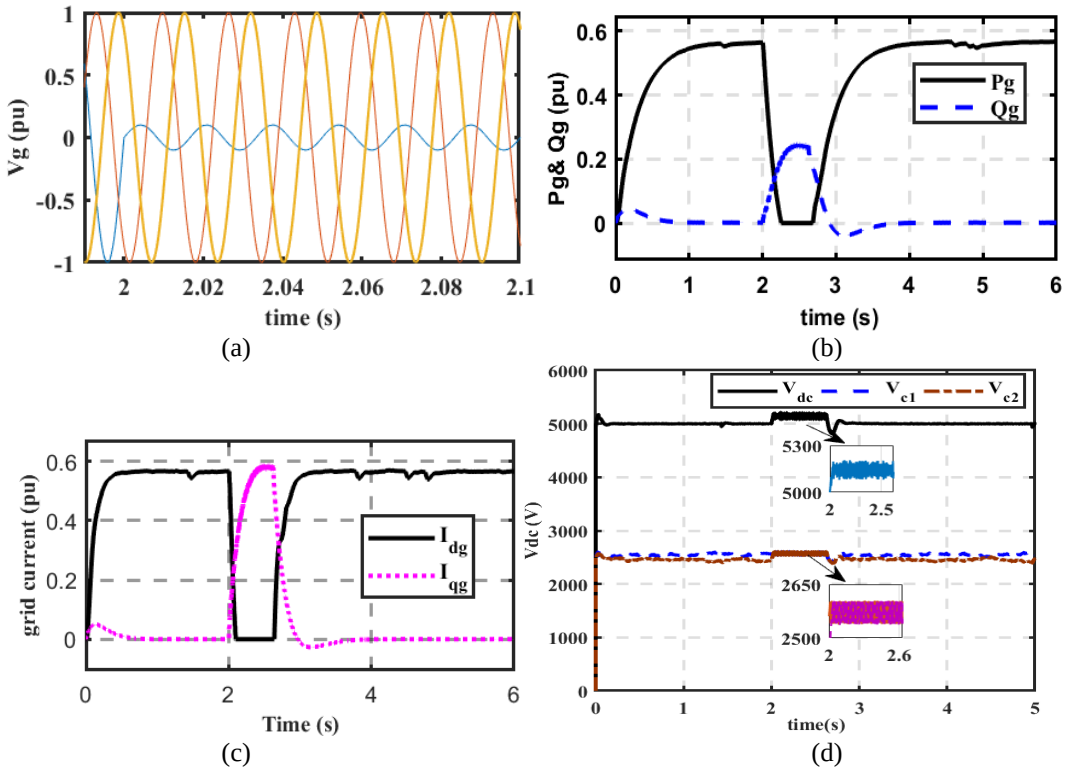


Figure. 11 Simulation results during asymmetrical three-phase grid voltage dip

## 5. Conclusion

This paper suggests a novel modulated model predictive control technique for the 3L-NPC power converter for WECS to overcome FCS-MPC algorithm difficulties. Low power ripples hence lower THD for PMSG current, is obtained when using a cost function with a time pattern and calculating the duty cycles from the selected voltage vector's cost functions. The PMSG stator current spectrum analysis ensures that the proposed MMPC scheme operates at fixed switching frequency during both steady-state and abnormal conditions. Also, the LVRT technique has the capability to recover the system performance during grid voltage fault, and the controller returns the system to its normal pre-fault condition quickly via injecting the WECS with the required reactive power. The results proved that the algorithm is stable and has a good response under different operating conditions. In future work, and due to the lack of experimental apparatus at this dramatic time, the validation of the proposed algorithm using the experimental tests is hereafter planned. The comparative results between MMPC and classical FCS-MPC show the effectiveness of the proposed MMPC in enhancing the results and reducing the simulation execution time and the computational effort associated with the calculation of the duty cycle of the converters also the total harmonic distortion (THD) has reduced by 31.34% lower than classical FCS-MPC and obtaining a constant switching frequency with a reduction in execution time by 51.17%. In addition, the comparative results of WECS during symmetrical and asymmetrical grid faults with and without LVRT controller show the effectiveness of LVRT controller in supporting the grid during faults and preventing the dc capacitor overvoltage despite the negative sequence component which appears during asymmetrical fault.

## Conflicts of Interest

The authors declare no conflict of interest

## Author Contributions

Conceptualization, A.A.G., E.G.S., A.-H.M.E. and A.A.Z.D.; methodology, A.A.G., E.G.S., A.-H.M.E. and A.A.Z.D.; software, A.A.G., E.G.S. and A.A.Z.D.; validation, A.A.G., E.G.S., and A.A.Z.D.; formal analysis, A.A.G., E.G.S., and A.A.Z.D.; investigation, E.G.S., Y.S.M., and A.A.Z.D.; resources, A.A.G., E.G.S., Y.S.M. and A.A.Z.D.; data curation, A.A.G., E.G.S., A.-H.M.E. and A.A.Z.D.; writing—original draft preparation, A.A.G., A.-H.M.E. and A.A.Z.D.; writing—review and editing, A.A.G., Y.S.M., and A.A.Z.D.; visualization, A.A.G. and A.A.Z.D.; administration, E.G.S., Y.S.M., A.-H.M.E. and A.A.Z.D. All authors have read and agreed to the published version of the manuscript.

## Acknowledgements

The research and publication of this article were performed as part of the employment of the authors at Minia University Egypt and Beni-Suef University Egypt.

## Notation list

| | |
|---|---|
| $v_w$ : wind speed in $(m/s)$ | $\lambda_T$ : tip speed ratio |
| β : pitch angle | $C_p$: power coefficient |
| $\rho$ : air density in $(kg/m^3)$, | A : rotor area in $(m^2)$ |
| $\omega_m$ : generator speed in $(rad/s)$ | $R_T$ : turbine rotor radius |
| $L_d, L_q, L_s$ : stator inductances | $X(k)$ : the stator current $i_{dq}(k)$ |
| $u(k)$ : the stator voltage $v_{dq}(k)$ | $A(k), B(k), H(k)$ : matrixes for PMSG parameters |
| $R_s, L_s$ : the stator resistance and inductance | $\varphi_m, \omega_e$ : flux linkage and electrical frequency |
| $T_s$ : sampling time | $u_x$ : voltage vector |
| $s_x, \overline{s}$ : switching state and it's complementary | $V_{dc}, i_{dc}$ : the dc link capacitor voltage and current. |
| $V_{c1}, V_{c2}$ : voltages of capacitors $c_1, c_2$ | $\lambda_{dc}$ : weighting factor |
| $i_\alpha^*, , i_\beta^*$ : reference stator current in stationary frame | $i_\alpha, i_\beta$ : actual stator current in stationary frame |

## References

[1] J. Carrasco, L. Franquelo, J. Bialasiewicz, and N. M. Alfonso, "Power-electronic systems for the grid integration of renewable energy sources: A survey", *IEEE Trans. Ind. Electron.*, Vol. 53, No. 4, pp. 1002-1016, 2006.

[2] F. Blaabjerg and K. Ma, "Future on power electronics for wind turbine systems", *IEEE J. Emerg. Sel. Top. Power Electron.*, Vol. 1, No. 3, pp. 139-152, 2013.

[3] Z. Zhenbin, "On control of grid-tied back-to-back power converters and permanent magnet

synchronous generator wind turbine systems", *Technische Universität München*, 2016.

[4] Z. Zhang, F. Wang, J. Wang, J. Rodríguez, and R. Kennel, "Nonlinear Direct Control for Three-Level NPC Back-to-Back Converter PMSG Wind Turbine Systems: Experimental Assessment with FPGA", *IEEE Trans. Ind. Informatics*, Vol. 13, No. 3, pp. 1172-1183, 2017.

[5] Z. Zhang, Z. Li, M. Kazmierkowski, J. Rodriguez, and R. Kennel, "Robust Predictive Control of Three-Level NPC Back-to-Back Power Converter PMSG Wind Turbine Systems with Revised Predictions", *IEEE Trans. Power Electron.*, Vol. 33, No. 11, pp. 9588-9598, 2018.

[6] M. Liserre, R. Cárdenas, M. Molinas, and J. Rodríguez, "Overview of multi-MW wind turbines and wind parks", *IEEE Trans. Ind. Electron.*, Vol. 58, No. 4, pp. 1081-1095, 2011.

[7] Z. Chen, J. Guerrero, and F. Blaabjerg, "A review of the state of the art of power electronics for wind turbines", *IEEE Trans. Power Electron.*, Vol. 24, No. 8, pp. 1859-1875, 2009.

[8] M. Ghanes, M. Trabelsi, H. A. Rub, and L. B. Brahim, "Robust Adaptive Observer-Based Model Predictive Control for Multilevel Flying Capacitors Inverter", *IEEE Trans. Ind. Electron.*, Vol. 63, No. 12, pp. 7876-7886, 2016.

[9] Q. Chen, X. Luo, L. Zhang, and S. Quan, "Model Predictive Control for Three-Phase", *IEEE Access*, Vol. 5, pp. 2834-2841, 2017.

[10] M. Rivera, M. P´erez, V. Yaramasu, and P. Wheeler, "Modulated model predictive control (M2PC) with fixed switching frequency for an NPC converter", In: *Proc. of Int. Conf. Power Eng. Energy Electr. Drives*, Vol. 2015-Septe, pp. 623-628, 2015.

[11] A. Olloqui, J. Elizondo, M. Rivera, and P. Wheeler, "Modulated model predictive rotor current control (M2PC) of a DFIG driven by an indirect matrix converter with fixed switching frequency", In: *Proc. of 2016 IEEE 2nd Annu. South. Power Electron. Conf. SPEC 2016*, 2016.

[12] R. Mikail, I. Husain, Y. Sozer, M. Islam, and T. Sebastian, "A fixed switching frequency predictive current control method for switched reluctance machines", *IEEE Trans. Ind. Appl.*, Vol. 50, No. 6, pp. 3717-3726, 2014.

[13] T. Wolbank, R. Stumberger, A. Lechner, and J. Machl, "A Novel Control Strategy for Optimal Inverter Switching Frequency Associated with Minimal Current Ripple Using Single Step Predictive Current Control", In: *Proc. of 13th Eur. Conf. Power Electron.*, pp. 1-9, 2009.

[14] M. Tomlinson, T. Mouton, R. Kennelt, U. V. Stellenbosch, and S. Africa, "Model predictive control with a fixed switching frequency for a 5-level flying capacitor converter", In: *Proc. of ECCE Asia Downunder, 2013 IEEE*, pp. 1208-1214, 2013.

[15] M. Tomlinson, T. Mouton, R. Kennel, and P. Stolze, "Model predictive control with a fixed switching frequency for an AC-to-AC converter", In: *Proc. of IEEE Int. Conf. Ind. Technol.*, pp. 570-575, 2013.

[16] M. Tomlinson, T. Mouton, R. Kennel, and P. Stolze, "A generic approach to implementing finite-set model predictive control with a fixed switching frequency", In: *Proc. of IEEE Int. Symp. Ind. Electron.*, Vol. 1, pp. 330-335, 2014.

[17] J. Hu and Z. Zhu, "Improved Voltage-vector sequences on dead-beat predictive direct power control of reversible three-phase grid-connected Voltage-source converters", *IEEE Trans. Power Electron.*, Vol. 28, No. 1, pp. 254-267, 2013.

[18] P. Antoniewicz and M. Kazmierkowski, "Virtual-flux-based predictive direct power control of AC/DC converters with online inductance estimation", *IEEE Trans. Ind. Electron.*, Vol. 55, No. 12, pp. 4381-4390, 2008.

[19] A. Damdoum, I. S. Belkhodja, M. P. David, and M. Debbou, "Low Voltage ride-through strategies for doubly fed induction machine pumped storage system under grid faults", *Renew. Energy*, Vol. 95, pp. 248-262, 2016.

[20] Z. Zheng, Q. Xie, C. Huang, X. Xiao, and C. Li, "Superconducting Technology Based Fault Ride Through Strategy for PMSG-Based Wind Turbine Generator: A Comprehensive Review", *IEEE Transactions on Applied Superconductivity*, Vol. 31, No. 8, pp. 1-6, 2021.

[21] M. Mahmoud, H. Salama, M. Aly, and A. M. A. Rahim, "Design and implementation of FLC system for fault ride-through capability enhancement in PMSG-wind systems", *Wind Engineering*, Vol. 45, No. 5, pp. 1361-1373, 2021.

[22] A. Loulijat, N. Ababssi, and M. Mohamed, "Kalman Observer Contribution to a Second Order Sliding Mode Control for Wind Turbine Based on DFIG During the Network Voltage Dip", *International Journal of Intelligent Engineering and Systems*, Vol. 14, No. 5, 2021, doi: 10.22266/ijies2021.1031.09.

[23] Z. Zhang, C. Hackl, and R. Kennel, "Computationally Efficient DMPC for Three-Level NPC Back-to-Back Converters in Wind Turbine Systems with PMSG", *IEEE Trans. Power Electron.*, Vol. 32, No. 10, pp. 8018-8034, 2017.

[24] C. Xia, S. Member, T. Liu, T. Shi, and Z. Song,

"A Simplified Finite-Control-Set Model-Predictive Control for Power Converters", *IEEE Trans. Ind. Informatics*, Vol. 10, No. 2, pp. 991-1002, 2014.

[25] G. Yang, H. Yi, C. Chai, B. Huang, Y. Zhang, and Z. Chen, "Predictive current control of boost three-level and T-type inverters cascaded in wind power generation systems", *Algorithms*, Vol. 11, No. 7, 2018.

[26] M. Tsili and S. Papathanassiou, "A review of grid code technical requirements for wind farms", *IET Renew. Power Gener.*, Vol. 3, No. 3, pp. 308-332, 2009.

[27] H. Geng, G. Yang, D. Xu, and B. Wu, "Unified power control for PMSG-based WECS operating under different grid conditions", *IEEE Trans. Energy Convers.*, Vol. 26, No. 3, pp. 822-830, 2011.

[28] A. Gencer, "Analysis and control of fault ride through capability improvement pmsg based on WECS using active crowbar system during different fault conditions", *Elektron. Ir Elektrotechnika*, Vol. 24, No. 2, pp. 63-69, 2018.

[29] C. Hackl, Z. Zhang, C. Hackl, M. Abdelrahem, and R. Kennel, "Voltage Sensorless Direct Model Predictive Control of 3L-NPC Back-to-Back Power Converter PMSG Wind Turbine Systems with Fast Dynamics Systems", *Tc (Clarke trans.)*, Vol. 3, No. April, 2016.